Available online at BIOMA: Jurnal Ilmiah Biologi
Websites:http://journal.upgris.ac.id/index.php/bioma/index
BIOMA: Jurnal Ilmiah Biologi, 15 (1), April 2026, 74-94
DOI: https://doi.org/10.26877/bioma.v15i1.3550

MORPHOLOGICAL CHARACTERIZATION OF BRAIN TUMOR TISSUE IN MRI IMAGES USING CNN AND TRANSFER LEARNING

Dafa Fadhilah Hilmi [1], Aji Prasetya Wibawa [1]*, Ardha Ardhana Putra Agustavada [1], Abdullah Sholum [1], Felix Andika Dwiyanto [2]

[1]*Informatics Engineering, Department of Electrical Engineering and Informatics, Universitas Negeri Malang*
Jl. Semarang 5, Malang City, East Java, Indonesia, 65145
[2]*Faculty of Computer Science, AGH University of Kraków*
al. Adama Mickiewicza 30, Kraków, Poland, 30-059
**Corresponding author: aji.prasetya.ft@um.ac.id*

ARTICLE INFO

Article history

Submission	2026-01-22
Revision	2026-03-09
Accepted	2026-04-14

Keywords:
Brain tumor
Deep learning
Magnetic resonance imaging
Neural tissue morphology
Pattern recognition

ABSTRACT

This study evaluates the role of computational pattern recognition as an observational method for analyzing morphological characteristics of brain tumor tissue in MRI data. A total of 6,056 labeled MRI images, including glioma, meningioma, and pituitary tumor cases, were examined. The images were standardized to maintain uniform structural representation and processed using three convolutional-based architectures: a baseline CNN, MobileNetV2, and EfficientNet-B0. Model performance was assessed using accuracy, precision, recall, F1-score, AUC-ROC, and a confusion matrix. The findings show variation in identification performance across tumor categories, with pituitary tumors consistently recognized, while misclassification predominantly occurred between glioma and meningioma. Models based on transfer learning achieved stronger agreement with the reference labels than the baseline CNN, with MobileNetV2 demonstrating the most stable performance. The recurrence of similar misclassification patterns across models suggests the presence of shared morphological characteristics in MRI representations of certain tumor types. Overall, the results support the use of computational image analysis as a structured observational framework that enables consistent evaluation of brain tumor tissue morphology in MRI, providing complementary insights for biological interpretation.

INTRODUCTION

Brain tumors represent pathological conditions of the central nervous system marked by uncontrolled cell growth that alters the structure and function of neural tissue. These structural changes affect neuronal signaling, physiological balance, and cognitive and motor functions. Each tumor category originates from distinct cellular sources within the brain, resulting in specific histological and morphological features. Gliomas develop from glial cells, meningiomas arise from the meninges, and pituitary tumors emerge from the pituitary gland. Differences in cellular origin lead to variation in lesion margins, infiltration patterns, and tissue architecture, which are significant in the context of human biology and health (Elmentaite et al., 2022). Despite these distinctions, certain tumor types display overlapping morphological characteristics in neural tissue, particularly regarding lesion boundaries and internal composition (Piotrzkowska Wróblewska et al., 2025). This resemblance complicates consistent assessment of tissue features. It indicates that differentiating tumor categories involves not only clinical evaluation but also biological interpretation of morphological patterns.

Direct examination of human brain tissue morphology under normal conditions is not possible; therefore, biological evaluation relies on indirect representations via imaging techniques. Magnetic Resonance Imaging (MRI) provides high-resolution visualization of soft tissue without exposure to ionizing radiation. It is a primary method for assessing neural tissue structure (Sack, 2022). The signals generated in MRI correspond to the tissue's physical characteristics, including proton density and water distribution. Differences in signal intensity and spatial configuration reflect variation in cellular composition, tissue density, and structural arrangement (Zhao et al., 2025). From this standpoint, MRI images function not only as radiological outputs but also as structured representations of biological tissue morphology.

Although MRI provides detailed structural information, image interpretation still relies heavily on clinicians' visual assessment. Such evaluation is influenced by individual expertise and becomes more challenging when different tumor types present similar structural features. Gliomas are frequently associated with diffuse, infiltrative margins, whereas meningiomas are generally well-circumscribed masses. Under specific imaging conditions, signal intensity overlaps and lesion boundaries may overlap, complicating accurate visual differentiation between the two. Lesions with comparable

margins and signal intensity patterns are often difficult to differentiate consistently through manual review (Yaqoob et al., 2023). This constraint indicates that interpreting neural tissue characteristics from imaging data requires complementary analytical support that delivers consistent, reproducible results.

Computational image analysis provides a method to assist biological observation by identifying structural patterns within visual data. Machine learning models based on Convolutional Neural Networks (CNN) can automatically extract spatial features from medical images (Mathi et al., 2025). Previous studies have largely concentrated on classification performance metrics. At the same time, relatively few have examined how detected patterns correspond to the tissue's biological characteristics (Ferguson et al., 2022). As a result, computational approaches are commonly presented as diagnostic systems rather than as analytical tools for studying tissue morphology.

A number of current approaches rely on intricate network architectures that demand significant computational power, which can constrain their application in iterative biological studies and in systematic image-based analyses (Ünal & Başçiftçi, 2022). Studies that apply image analysis specifically to investigate morphological differences in neural tissue among various tumor categories are still relatively scarce. Moreover, the potential of recurring misclassification patterns as a basis for interpreting structural similarities across tumor categories remains insufficiently explored. As a result, the role of computational pattern recognition in advancing understanding of structural variation within brain tissue has yet to be fully examined.

Considering these aspects, this research specifically positions computational image analysis as an investigative approach for examining static biological tissue morphology in MRI images. The central argument is that MRI scans should be interpreted as biological data reflecting neural tissue structure, and that machine learning can consistently identify underlying structural patterns relevant to tumor categorization. The study analyzes 6,056 human brain MRI images, categorized into glioma, meningioma, and pituitary tumors, to assess cross-sectional morphological differences in tumor appearance (Bahuguna et al., 2023). Unlike previous work focused just on classification accuracy, this investigation contrasts a baseline CNN architecture with MobileNetV2 and EfficientNet-B0 transfer learning models to assess the reliability of recognition and misclassification patterns. The

explicit aim is to illuminate structural similarities and differences rather than solely ranking model performance.

This study aims to clarify how computational pattern recognition can reveal cross-sectional morphological variation in human brain tumor tissue through MRI-based representations. The main argument is that repeated recognition outcomes, such as misclassification trends observed with established convolutional neural networks, can reveal structural similarities among brain tumor categories. The computational method is designed to support, not replace, clinical diagnostic procedures by making morphological similarities and differences more evident across different model configurations. Highlighting classification errors as informative signals, the study positions computational pattern recognition as an analytical tool for interpreting tissue morphology rather than merely evaluating model accuracy. This reframing is anticipated to support image-driven analysis as a complementary strategy for investigating tissue structure and assessing human health.

MATERIALS AND METHODS

This section describes the data sources and methods used to study differences in human brain tumor tissue. MRI scans represented neural structures. Computational techniques enabled systematic analysis. Each method preserved biological information while ensuring consistent detection of tissue features. Every step, from data preparation to evaluation, took place under controlled conditions for reliable interpretation.

Dataset and Biological Material

The study used the publicly available Bangladesh Brain Tumor MRI Dataset. The images came from multiple hospitals in Bangladesh (Rahman, 2024). The documentation does not specify how many hospitals participated. Before analysis, images were checked manually for quality and labeling. In total, 6,056 MRI images were chosen. They were divided into three groups: 2,004 with glioma, 2,004 with meningioma, and 2,048 with pituitary tumors. These groups represent different origins and locations in the brain. Gliomas start in glial cells in the brain tissue. Meningiomas grow from the layers of the meninges. Pituitary tumors form in the pituitary region

(Pichaivel et al., 2022). This grouping enabled comparison of growth patterns among the tumor types.

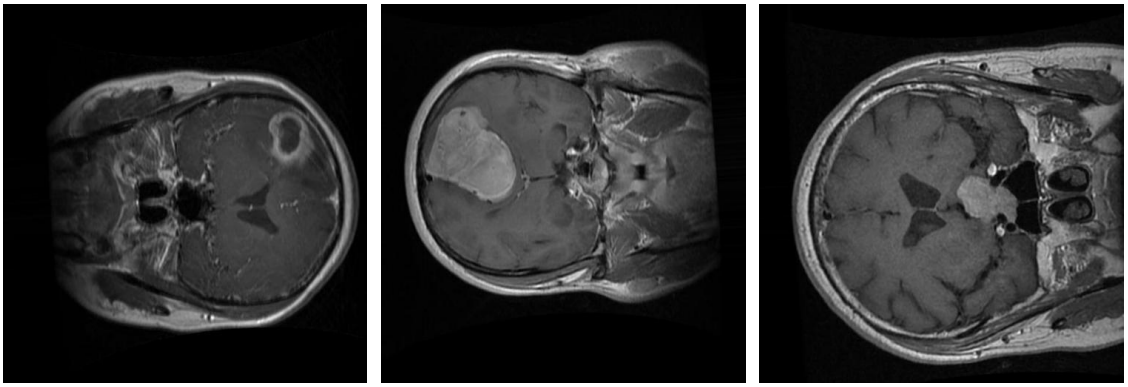

(a) (b) (c)

Figure 1. Representative brain MRI images illustrating distinct morphological characteristics of tumor tissue: (a) glioma with diffuse and infiltrative boundaries, (b) meningioma with relatively well-defined mass structure, and (c) pituitary tumor with localized and compact morphology

Figure 1 displays sample MRI scans from the three tumor categories to highlight observable differences in tissue architecture and lesion features across tumor types. The images reveal variation in lesion margin clarity, internal signal heterogeneity, and anatomical positioning before computational processing is applied. Glioma cases are commonly characterized by irregular, diffuse lesion margins accompanied by heterogeneous signal intensity, reflecting their infiltrative growth within brain tissue. In contrast, meningioma images tend to display more clearly delineated boundaries, forming mass-like structures adjacent to the meningeal layer, although variations in internal texture may still be observed. Meanwhile, pituitary tumors are generally identified as localized and compact formations within the sellar region, often exhibiting more uniform signal intensity patterns (Resende & Alves, 2021). These observable features serve as the foundation for subsequent pattern recognition procedures aimed at achieving consistent identification of tissue morphology.

All MRI scans were saved in JPG format with an initial spatial resolution of 512 × 512 pixels. The images were presented in grayscale, where pixel intensity represented differences in tissue signal properties. Variations in MRI intensity correspond to physical tissue attributes, such as proton density and water distribution, enabling the visualization of soft tissue structures (Zhao et al., 2025). Differences in intensity values

are therefore associated with biological characteristics of brain tissue, such as tissue density and internal structural organization (Bianchi et al., 2022). In this grayscale format, structural details of lesion margins, internal heterogeneity, and adjacent tissue arrangement were preserved, enabling the images to serve as observational data for examining morphological features of brain tumor tissue.

Hardware and Software

All computational procedures were executed on the Google Colaboratory cloud platform. Model training and evaluation were accelerated using an NVIDIA Tesla T4 GPU available in this environment, while access to the platform was via a personal computer running Windows 11. Data processing and model development were implemented in Python. The deep learning models were constructed using the TensorFlow framework with the Keras API, based on the default library configuration provided in Google Colaboratory during the experimental period.

Several supporting libraries were employed to facilitate analysis. NumPy handled numerical computations, OpenCV was used for image preprocessing, Scikit-learn for computing classification performance metrics, and Matplotlib for visualizing training progress and classification results. The same computational setup was maintained across training, validation, and testing to ensure consistent analytical execution.

Image Standardization

Before computational analysis, the MRI scans were standardized to achieve a consistent representation of tissue structure across the dataset. Differences in acquisition parameters and subject positioning can alter visual characteristics; therefore, a normalization step was implemented to reduce variation unrelated to biological factors (Abbasi et al., 2024). Each image was rescaled from its initial resolution of 512 × 512 pixels to 224 × 224 pixels. This modification preserved spatial proportions while ensuring uniform input dimensions for further processing. The resizing operation was applied uniformly to all samples, ensuring that any detected variation corresponded to tissue properties rather than differences in image scale.

In this study, MRI data were represented as two-dimensional slices, with each image corresponding to a single cross-sectional slice of brain tissue. By comparison, three-dimensional MRI constructs a continuous volumetric representation by combining

sequential slices, allowing spatial relationships within the brain to be captured more comprehensively (Woo & Lee, 2021). The selection of two-dimensional images in this work supported a standardized data format and enabled consistent preprocessing procedures, while still preserving key visual features relevant to tissue morphology.

Following resizing, intensity normalization was applied to limit the variation introduced by imaging conditions. MRI signal levels may differ due to acquisition settings and scanner calibration, even when tissue composition remains comparable (Wahid et al., 2021). The normalization process adjusted intensity ranges across all images while maintaining relative contrast between lesion regions and adjacent tissue, ensuring that structural patterns linked to tissue morphology remained distinguishable. To address variation in head positioning during image acquisition, controlled rotation was introduced within the training dataset. This transformation simulated differences in anatomical orientation without modifying inherent tissue structure. As described by (Darzi & Bocklitz, 2024), such an approach supports the recognition of morphological features independent of orientation while preserving underlying biological information.

Although the initial MRI scans were in grayscale, they were converted to a three-channel format required by the convolutional network. The identical pixel values were duplicated across all channels, ensuring that no new visual information was added and that the biological content remained intact. Following the standardization stage, the dataset was partitioned into training, validation, and testing groups with a proportion of 60:20:20. The training data were used to learn characteristics of tissue patterns, the validation data monitored consistency during the recognition process, and the testing data functioned as an independent set to assess pattern identification on images not previously included in model development (Tampu et al., 2022).

Computational Analysis

Identification of tissue morphology patterns was conducted using convolutional-based recognition architectures. The study evaluated three configurations, a baseline CNN and two transfer learning approaches, MobileNetV2 and EfficientNet-B0. CNNs are commonly used in medical image analysis because they can extract spatial features directly from visual inputs (Gu, 2024). These architectures were chosen to assess the stability of structural pattern recognition across varying levels of feature representation.

The baseline CNN architecture was designed to extract fundamental spatial features directly from MRI inputs. Its convolutional layers captured localized image attributes, including edge contrast and regional intensity differences, which reflect variation in tissue organization (Khan et al., 2022). In contrast, the transfer learning approaches incorporated pretrained weights obtained from the ImageNet dataset. This strategy allows visual features learned from large-scale datasets to be adapted to new imaging contexts, thereby contributing to greater stability in medical image pattern recognition (Jayabharathi S & Dr. V. Ilango, 2025). In these models, the backbone network served as a fixed feature extractor, while the final classification layer was modified to classify into the three tumor classes. Training was applied only to the classification layer using the MRI dataset.

The three model configurations were chosen to reflect varying degrees of computational feature extraction. A baseline CNN was implemented to capture fundamental spatial patterns derived directly from the MRI data, while MobileNetV2 and EfficientNet-B0 were employed to assess the stability of recognition patterns generated by pretrained feature extractors. This comparative design focused on evaluating the consistency of morphological pattern detection and the distribution of classification errors across different computational representations, rather than solely comparing predictive accuracy among models.

To explain the functional contribution of each computational configuration in observing morphology, the conceptual distinctions among the models are outlined in Table 1. These architectures correspond to varying depths of feature representation, extending from basic structural patterns to more refined morphological details.

Table 1. Conceptual roles of computational models used for tissue morphology observation

Aspect	CNN Sequential	MobileNetV2	EfficientNet-B0
Model approach	Reference recognition model	Transfer learning-based recognition	Transfer learning-based recognition
Primary role	Observation of primary structural tissue patterns	Consistent identification of tumor morphology	Identification of subtle structural variation
Initial weight source	Trained on the MRI dataset	Pretrained weights (ImageNet)	Pretrained weights (ImageNet)
Feature extraction strategy	Fully trainable convolutional layers	Frozen backbone as feature extractor	Frozen backbone as feature extractor

Aspect	CNN Sequential	MobileNetV2	EfficientNet-B0
		with retrained classifier	with retrained classifier
Regularization method	Not applied	Dropout regularization	Dropout regularization
Intended purpose	Reference model for basic tissue pattern observation	Stable recognition of tumor tissue morphology	Detection of fine morphological characteristics

Model training used the Adam optimization algorithm with a categorical cross-entropy loss function. Adam is widely used in deep learning because it adapts parameter updates throughout the training process (Ismail et al., 2025). All models were trained using the same parameter configuration, while the number of epochs ranged from 10 to 50 to ensure controlled experimental conditions. Throughout the training process, validation data were regularly monitored to track recognition patterns and to minimize overfitting in the identification of tissue characteristics. The comparison across these model setups aimed to assess whether brain tumor morphology could be consistently recognized using different feature extraction approaches, as well as to evaluate whether repeated misclassification trends indicated similarities in MRI-derived tissue representations.

Evaluation and Data Analysis

The evaluation phase aimed to measure the stability of morphological pattern recognition in brain tumor tissue. Labels generated by the classification system were matched against reference annotations through a confusion matrix. This procedure enabled analysis of correspondence and mismatch between detected structural patterns and established tumor categories. The confusion matrix included four elements, namely true positive (TP), true negative (TN), false positive (FP), and false negative (FN), which represent correct and incorrect classification outcomes (Kunta & Lepakshi, 2024). These components were then used to derive multiple quantitative performance metrics.

$$Accuracy = \frac{TP + TN}{TP + TN + FP + FN} \quad \text{(I)}$$

$$Precision = \frac{TP}{TP + FP} \quad \text{(II)}$$

$$Recall = \frac{TP}{TP + FN} \quad \text{(III)}$$

$$F1 - Score = 2 \times \frac{Precision \times Recall}{Precision + Recall} \quad \text{(IV)}$$

Accuracy quantified the proportion of images for which the predicted tissue category matched the reference annotation. Precision reflected the consistency of predictions when a particular tumor class was assigned. In contrast, recall measured the system's ability to identify all cases in the dataset belonging to a given tumor category. The F1-score combines precision and recall into a single metric, offering a balanced assessment of prediction reliability and detection coverage (Durga & Godavarthi, 2024). In the context of biological assessment, recall was particularly important because undetected tumor categories indicated that the system did not capture relevant structural tissue features. Precision indicated how closely the predicted patterns matched the actual tissue morphology (Jang et al., 2021). The joint interpretation of these metrics allowed examination of the consistency with which morphological characteristics were differentiated across tumor classes.

The Area Under the Receiver Operating Characteristic Curve, or AUC-ROC, was also computed to assess the separation of probability distributions among tumor categories at various classification thresholds. Elevated AUC-ROC values reflected clearer distinction of tissue morphology patterns (Teferi & Akinyemi, 2024). All performance measures were derived from an independent testing dataset excluded from the training phase. This separation ensured that the outcomes reflected generalization in tissue pattern recognition rather than the retention of training samples. Consequently, the evaluation assessed the reliability of computational observation in identifying morphological features of brain tumor tissue.

RESULTS AND DISCUSSION

This study analyzed the ability of computational pattern recognition to extract structural characteristics of brain tumor tissue from MRI data. The first phase focused on assessing model performance during both training and validation to ensure that predictions were driven by learned visual patterns rather than by the retention of individual samples. In every configuration tested, the training loss declined gradually, while the validation loss stabilized as training progressed. The parallel pattern observed

between the training and validation metrics indicated consistent, stable learning throughout model development.

Once training was completed, each model was tested using an independent dataset to assess tumor category identification. The results indicated that tumor types with well-defined structural boundaries were classified more consistently. In contrast, tumor types with comparable visual characteristics caused greater confusion. The quantitative performance outcomes derived from this testing phase are presented in Table 2.

Table 2. Optimal Performance Comparison of Brain Tumor Classification Models

Architecture Model	Epoch	Accuracy	Precision	Recall	F1-Score	AUC-ROC
CNN	20	0.82	0.82	0.82	0.82	0.9421
MobileNetV2	50	0.96	0.96	0.96	0.96	0.9959
EfficientNet-B0	50	0.95	0.95	0.95	0.95	0.9921

The identification results obtained from the testing dataset are summarized in Table 2. The quantitative indicators were calculated to measure the consistency of tissue category recognition across the evaluated model configurations. These metrics provide an overall description of how closely the predicted labels matched the reference annotations for each tumor category. By presenting accuracy, precision, recall, F1-score, and AUC-ROC values together, the table allows comparison of identification agreement and category separation across the different model approaches.

Table 2 shows that all models identified tumor tissue categories, though with varying levels of agreement with the reference labels. The baseline CNN model achieved an accuracy value of 0.82, whereas the transfer learning models showed higher agreement. MobileNetV2 reached an accuracy of 0.96, and EfficientNet-B0 achieved 0.95. The findings suggest that convolutional neural network architectures are effective in capturing and recognizing structural characteristics of brain tumor tissue from MRI data. Among the tested configurations, MobileNetV2 showed the strongest alignment with the reference annotations, resulting in the most consistent identification performance in this study.

A similar pattern appeared in the precision, recall, and F1-score values. The CNN model produced balanced but lower values across categories. In contrast, both transfer learning models showed higher and more consistent identification across all indicators. The AUC-ROC values also demonstrated improved category separation, with

MobileNetV2 obtaining 0.9959 and EfficientNet-B0 obtaining 0.9921, compared with 0.9421 for the baseline CNN model.

Although the quantitative metrics describe overall identification performance, they do not indicate how the predictions were distributed among tumor categories. Therefore, the classification outcomes for each model are further examined using the confusion matrices presented in Figures 2-4.

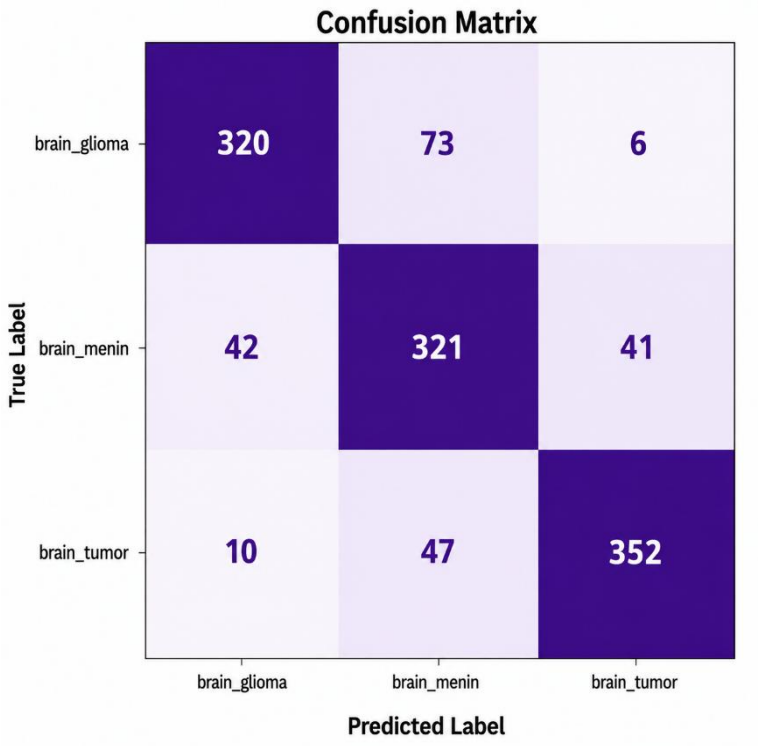

Figure 2. Confusion matrix of the baseline CNN model in the best scenario for the classification of brain tumor MRI images

The distribution of classification outcomes for the baseline CNN model is presented in Figure 2. The confusion matrix shows that correct identification occurred across all tumor categories; however, disagreement between predicted and reference labels persisted.

For glioma, 320 samples were correctly identified, while 73 were classified as meningioma and 6 as pituitary tumor. For meningioma, 321 samples were correctly recognized, whereas 42 were predicted as glioma and 41 as pituitary tumor. The pituitary tumor category had the highest number of correct identifications, with 352 samples correctly classified. At the same time, 47 were predicted to be meningiomas and 10 to be gliomas.

The misclassification pattern was not uniformly distributed among categories. Most incorrect predictions occurred between glioma and meningioma, while fewer errors involved the pituitary tumor category. These results show that disagreement between predicted labels was concentrated in specific category pairs rather than randomly distributed across all classes.

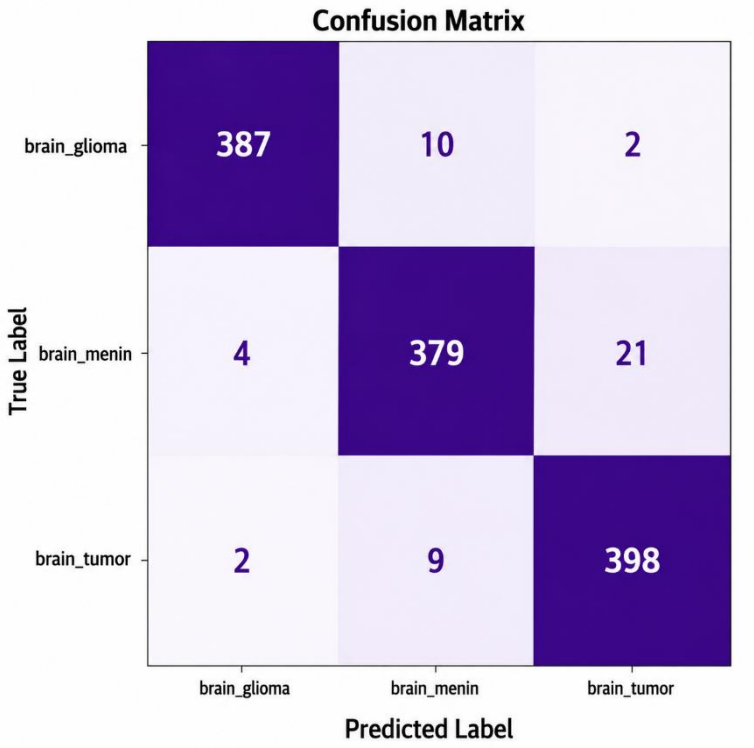

Figure 3. Confusion matrix of the MobileNetV2 model in the best scenario for the classification of brain tumor MRI images

Figure 3 displays the classification distribution produced by the MobileNetV2 model. When contrasted with the baseline CNN, a greater share of samples was assigned to the correct tumor class across all categories. Predictions that matched the reference annotations increased, while discrepancies between predicted and actual labels were reduced. This pattern shows greater consistency between model outputs and the annotated tumor categories across the test dataset.

Within the glioma group, 387 images were assigned to the correct class, while 10 were labeled as meningioma and 2 as pituitary tumor. For meningioma cases, 379 samples matched the reference category, with 4 misclassified as glioma and 21 as pituitary tumor. The pituitary tumor class demonstrated the strongest agreement, with 398 images correctly identified and only a limited number allocated to other categories.

Overall, the misclassification frequency decreased compared with the baseline CNN. Confusion between glioma and meningioma persisted, although it occurred less often. The pituitary tumor category continued to show the highest consistency, reflected by the lowest proportion of disagreement relative to the reference annotations.

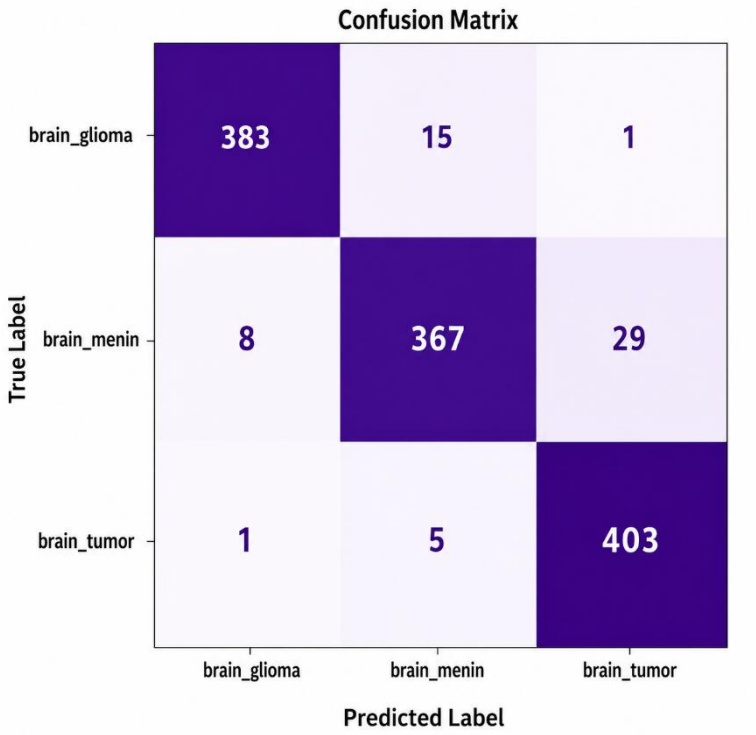

Figure 4. Confusion matrix of the EfficientNet-B0 model in the best scenario for the classification of brain tumor MRI images

Figure 4 presents the classification results generated by the EfficientNet-B0 model. Accurate predictions were obtained across all tumor categories, with most samples aligning with their respective reference labels. Despite this overall agreement, some category pairs continued to exhibit misclassification. The majority of predictions were located along the main diagonal of the confusion matrix, indicating concordance with the annotated labels. In contrast, a limited number of entries appeared outside the diagonal, indicating discrepancies between predicted and actual tumor classes.

Among the glioma cases, 326 samples were correctly classified, while 61 were assigned to the meningioma category and 12 to the pituitary tumor. For meningioma, 279 images matched the reference label, whereas 76 were predicted as glioma and 49 as pituitary tumor. The pituitary tumor group again recorded the highest number of correct

classifications, with 350 samples correctly identified and fewer misclassifications than in the other categories.

Although all tumor types were recognized, the distribution of errors followed a specific pattern rather than occurring randomly. Misclassification was concentrated mainly between glioma and meningioma, while pituitary tumors exhibited lower levels of confusion with the remaining categories. This pattern of disagreement between particular tumor pairs was consistently observed across the evaluated model configurations.

Referring to the findings summarized in Table 2, the confusion matrix shows that classification performance differs across tumor categories and is not random. The pituitary tumor group consistently recorded the highest proportion of correct predictions across all assessed models, whereas misclassifications were predominantly between glioma and meningioma. This repeated pattern indicates that the recognition mechanism relies on visual characteristics embedded in the MRI images rather than on arbitrary tumor labeling.

Pituitary tumors were identified with greater consistency because they arise in a distinct anatomical location and commonly present as well-localized masses. On MRI scans, these lesions are often clearly separated from adjacent brain tissue, which facilitates recognition of their boundaries. In contrast, gliomas tend to infiltrate the surrounding brain parenchyma and display heterogeneous signal intensity (Hu et al., 2024), which reduces visual separation between the lesion and nearby structures. Meningiomas arise from the meningeal layer and typically appear as surface-based masses; however, in certain imaging views, their internal signal characteristics and margins may resemble those of gliomas (Damalcheruvu et al., 2022). These structural features account for the repeated misclassification between the glioma and meningioma categories (Boaro et al., 2022).

The recurrence of comparable misclassification patterns across multiple model architectures indicates that the constraint was linked to the imaging representation rather than to differences in computational design (Patrício et al., 2024). The results show that CNN architectures can effectively capture the structural patterns of brain tumor tissue from MRI data. Among the tested models, MobileNetV2 achieved the best results, suggesting that lightweight transfer learning approaches can deliver stable feature

extraction and reliable class separation. From a biological standpoint, the recurrent misclassification between glioma and meningioma indicates overlapping morphological features in their MRI appearances, which may constrain accurate differentiation when relying solely on visual structural characteristics. Even with more advanced architectures, several samples remained difficult to distinguish. These findings are consistent with previous reports that pretrained feature extractors improve medical image recognition by capturing edge structures, contrast differences, and textural organization (Valverde et al., 2021).

From a biological standpoint, the findings suggest that computational image analysis is a useful tool for examining static tissue characteristics visible in MRI scans. The present framework evaluates structural features captured at a single imaging time point and therefore should not be interpreted as a direct measure of temporal tumor development. The system is not intended to substitute clinical interpretation but to assist by identifying areas that warrant more detailed assessment. In practical settings, this method can facilitate initial image screening, enabling clinicians to focus on scans that exhibit ambiguous structural features for subsequent evaluation (Imran et al., 2024).

This study has several limitations. The analysis was restricted to two-dimensional MRI slices, in which each image represents a single cross-sectional view of brain tissue. Variations in slice orientation and acquisition settings can affect how tissue structures appear, and the model does not account for three-dimensional spatial continuity within the brain (Zhou et al., 2022). Three-dimensional MRI integrates information from consecutive slices to represent spatial relationships more completely, enabling a clearer depiction of tumor extent and structural continuity, aspects that are not fully captured in the current analysis. Furthermore, the dataset was limited to single MRI examinations, which prevented assessment of temporal tumor progression, including volumetric expansion, recurrence, infiltration dynamics, or structural alterations related to treatment. While longitudinal MRI can be applied to observe these changes over time, such temporal evaluation was not included in this study and should be explored in future research using sequential MRI datasets. Furthermore, the dataset lacked histopathological verification for each sample. As a result, the evaluation focused on imaging representation rather than confirmed pathological diagnosis. Differences in MRI acquisition protocols across data

sources may also introduce variation in signal intensity despite the applied standardization procedures (Bhattacharjee et al., 2023).

Future studies should integrate volumetric MRI datasets to better represent the three-dimensional continuity of brain tissue structures. Incorporating such data would allow examination of spatial relationships across adjacent slices and could enhance the interpretation of tumor morphology, especially in cases involving infiltrative growth that spans multiple regions. The inclusion of multiple imaging modalities, such as T1-, T2-, and FLAIR-weighted sequences, may provide complementary structural detail and improve tumor type separation (Vieira de Mello et al., 2021). Further work can also integrate imaging findings with clinical records or histopathological evidence to establish stronger links between image-based patterns and underlying biological tissue properties. In addition, explainable analysis methods can be implemented to identify specific image regions that influence classification outcomes, thereby enabling clearer interpretation of the tissue characteristics detected (Chen et al., 2025).

The results of this study indicate that computational pattern recognition can serve as a supportive analytical method for examining morphological features of brain tumor tissue in MRI scans. This approach offers a structured framework for assessing structural patterns that are challenging to evaluate consistently through visual observation alone. By identifying regions associated with uncertain predictions and recurring classification discrepancies, the analysis highlights areas within the imaging data that require closer review. The proposed system is not designed to substitute clinical diagnosis, but to complement it by assisting in the assessment of structural patterns and facilitating biological and clinical interpretation.

CONCLUSION

This research analyzed brain tumor MRI scans through computational pattern recognition to investigate morphological features of neural tissue. The findings revealed variation in identification performance across tumor types. Pituitary tumors were classified with high consistency, whereas discrepancies occurred predominantly between glioma and meningioma categories. These results suggest that some tumor tissues exhibit

MRI features that are comparable, complicating differentiation based on structural appearance.

This study contributes by applying deep learning-derived recognition patterns to facilitate the biological interpretation of tumor tissue morphology. Instead of viewing classification errors solely as technical shortcomings, recurring misclassification trends are analyzed as signals of morphological similarity among tumor categories in MRI data. The findings suggest that computational image analysis serves as a supportive observational tool for examining tissue structure, rather than replacing clinical diagnostic processes. Through this approach, structural patterns in imaging data can be systematically evaluated, supporting the initial assessment of brain tumor MRI scans and the biological interpretation of tissue characteristics.

REFERENCES

Abbasi, S., Lan, H., Choupan, J., Sheikh-Bahaei, N., Pandey, G., & Varghese, B. (2024). Deep learning for the harmonization of structural MRI scans: a survey. *BioMedical Engineering OnLine*, *23*(1), 90. https://doi.org/10.1186/s12938-024-01280-6

Bahuguna, A., Ashraf, A., Kavita, Verma, S., & Negi, P. (2023). *Brain Tumor Classification from MRI Scans* (pp. 713–725). https://doi.org/10.1007/978-981-99-3010-4_57

Bhattacharjee, B., Debnath, B., Chandra Das, J., & De, D. (2023). *Isolating Brain Tissue from Abnormal Tissue Using MRI-Based U-Net Convolutional Neural Network* (pp. 721–728). https://doi.org/10.1007/978-981-99-3656-4_74

Bianchi, L., Cavarzan, F., Ciampitti, L., Cremonesi, M., Grilli, F., & Saccomandi, P. (2022). Thermophysical and mechanical properties of biological tissues as a function of temperature: a systematic literature review. *International Journal of Hyperthermia*, *39*(1), 297–340. https://doi.org/10.1080/02656736.2022.2028908

Boaro, A., Kaczmarzyk, J. R., Kavouridis, V. K., Harary, M., Mammi, M., Dawood, H., Shea, A., Cho, E. Y., Juvekar, P., Noh, T., Rana, A., Ghosh, S., & Arnaout, O. (2022). Deep neural networks allow expert-level brain meningioma segmentation and present potential for improvement of clinical practice. *Scientific Reports*, *12*(1), 15462. https://doi.org/10.1038/s41598-022-19356-5

Chen, Y., Lin, H., Sun, J., Pu, R., Zhou, Y., & Sun, B. (2025). Texture Feature Differentiation of Glioblastoma and Solitary Brain Metastases Based on Tumor and Tumor-brain Interface. *Academic Radiology*, *32*(1), 400–410. https://doi.org/10.1016/j.acra.2024.08.025

Damalcheruvu, P. R., Mian, M., Sharma, S., Patro, S., Vattoth, S., Viswamitra, S.,

Ramakrishnaiah, R. H., Kumar, M., & Van Hemert, R. L. (2022). Meningioma or Mimic: Look Twice and Save a Life. *Neurographics*, *12*(4), 216–232. https://doi.org/10.3174/ng.2100061

Darzi, F., & Bocklitz, T. (2024). A Review of Medical Image Registration for Different Modalities. *Bioengineering*, *11*(8), 786. https://doi.org/10.3390/bioengineering11080786

Durga, P., & Godavarthi, D. (2024). A deep learning-based intelligent decision-making model for tumor and cancer cell identification. *Bulletin of Electrical Engineering and Informatics*, *13*(1), 510–518. https://doi.org/10.11591/eei.v13i1.6469

Elmentaite, R., Domínguez Conde, C., Yang, L., & Teichmann, S. A. (2022). Single-cell atlases: shared and tissue-specific cell types across human organs. *Nature Reviews Genetics*, *23*(7), 395–410. https://doi.org/10.1038/s41576-022-00449-w

Ferguson, D., Henderson, A., McInnes, E. F., Lind, R., Wildenhain, J., & Gardner, P. (2022). Infrared micro-spectroscopy coupled with multivariate and machine learning techniques for cancer classification in tissue: a comparison of classification method, performance, and pre-processing technique. *The Analyst*, *147*(16), 3709–3722. https://doi.org/10.1039/D2AN00775D

Gu, C. (2024). Enhancing medical image classification with convolutional neural networks through transfer learning: A comprehensive review. *Applied and Computational Engineering*, *35*(1), 280–284. https://doi.org/10.54254/2755-2721/35/20230407

Hu, B., Zhang, Z., Chen, S., Xu, Q., & Li, J. (2024). A metric for quantitative evaluation of glioma margin changes in magnetic resonance imaging. *Acta Radiologica*, *65*(6), 645–653. https://doi.org/10.1177/02841851241229597

Imran, M. T., Shafi, I., Ahmad, J., Butt, M. F. U., Villar, S. G., Villena, E. G., Khurshaid, T., & Ashraf, I. (2024). Virtual histopathology methods in medical imaging - a systematic review. *BMC Medical Imaging*, *24*(1), 318. https://doi.org/10.1186/s12880-024-01498-9

Ismail, A. R., Azhary, M. Z. R., & Hitam, N. A. (2025). *Evaluating Adan vs. Adam: An Analysis of Optimizer Performance in Deep Learning* (pp. 251–263). https://doi.org/10.1007/978-3-031-82931-4_19

Jang, H.-J., Song, I. H., & Lee, S. H. (2021). Generalizability of Deep Learning System for the Pathologic Diagnosis of Various Cancers. *Applied Sciences*, *11*(2), 808. https://doi.org/10.3390/app11020808

Jayabharathi S, & Dr.V.Ilango. (2025). Transfer Learning Models in Medical Image Anomaly Detection. *International Journal of Scientific Research in Science and Technology*, *12*(2), 1186–1189. https://doi.org/10.32628/IJSRST251222678

Khan, S., Azam, B., Yao, Y., & Chen, W. (2022). Deep collaborative network with alpha matte for precise knee tissue segmentation from MRI. *Computer Methods and Programs in Biomedicine*, *222*, 106963.

https://doi.org/10.1016/j.cmpb.2022.106963

Kunta, J. P. K. C., & Lepakshi, V. A. (2024). Enhancing Breast Cancer Detection Through a Tailored Convolutional Neural Network Deep Learning Approach. *SN Computer Science*, *5*(7), 826. https://doi.org/10.1007/s42979-024-03197-2

Mathi, S., Deb, D., Chaudhuri, A. K., Joseph, L., & Biswas, S. (2025). A Review Of Convolutional Neural Networks For Medical Image Analysis: Trends And Future Directions. *Journal of Neonatal Surgery*, *14*(7), 90–97. https://doi.org/10.63682/jns.v14i7.5117

Patrício, C., Neves, J. C., & Teixeira, L. F. (2024). Explainable Deep Learning Methods in Medical Image Classification: A Survey. *ACM Computing Surveys*, *56*(4), 1–41. https://doi.org/10.1145/3625287

Pichaivel, M., Anbumani, G., Theivendren, P., & Gopal, M. (2022). An Overview of Brain Tumor. In *Brain Tumors*. IntechOpen. https://doi.org/10.5772/intechopen.100806

Piotrzkowska Wróblewska, H., Karwat, P., Żyłka, A., Dobruch Sobczak, K., Dedecjus, M., & Litniewski, J. (2025). Quantitative Ultrasound-Based Precision Diagnosis of Papillary, Follicular, and Medullary Thyroid Carcinomas Using Morphological, Structural, and Textural Features. *Cancers*, *17*(17), 2761. https://doi.org/10.3390/cancers17172761

Rahman, M. M. (2024). Brain Cancer - MRI dataset. In *Mendeley Data*. Mendeley Data. https://doi.org/10.17632/mk56jw9rns.1

Resende, L. L., & Alves, C. A. P. F. (2021). Imaging of brain tumors in children: the basics—a narrative review. *Translational Pediatrics*, *10*(4), 1138–1168. https://doi.org/10.21037/tp-20-285

Sack, I. (2022). Magnetic resonance elastography from fundamental soft-tissue mechanics to diagnostic imaging. *Nature Reviews Physics*, *5*(1), 25–42. https://doi.org/10.1038/s42254-022-00543-2

Tampu, I. E., Eklund, A., & Haj-Hosseini, N. (2022). Inflation of test accuracy due to data leakage in deep learning-based classification of OCT images. *Scientific Data*, *9*(1), 580. https://doi.org/10.1038/s41597-022-01618-6

Teferi, M. B., & Akinyemi, L. A. (2024). Deep Learning-Based Cross-Cancer Morphological Analysis: Identifying Histopathological Patterns in Breast and Lung Cancer. *Journal of Future Artificial Intelligence and Technologies*, *1*(3), 235–248. https://doi.org/10.62411/faith.3048-3719-36

Ünal, H. T., & Başçiftçi, F. (2022). Evolutionary design of neural network architectures: a review of three decades of research. *Artificial Intelligence Review*, *55*(3), 1723–1802. https://doi.org/10.1007/s10462-021-10049-5

Valverde, J. M., Imani, V., Abdollahzadeh, A., De Feo, R., Prakash, M., Ciszek, R., & Tohka, J. (2021). Transfer Learning in Magnetic Resonance Brain Imaging: A

Systematic Review. *Journal of Imaging*, *7*(4), 66. https://doi.org/10.3390/jimaging7040066

Vieira de Mello, J. P., Paixao, T. M., Berriel, R., Reyes, M., Badue, C., De Souza, A. F., & Oliveira-Santos, T. (2021). Deep Learning-based Type Identification of Volumetric MRI Sequences. *2020 25th International Conference on Pattern Recognition (ICPR)*, 1–8. https://doi.org/10.1109/ICPR48806.2021.9413120

Wahid, K. A., He, R., McDonald, B. A., Anderson, B. M., Salzillo, T., Mulder, S., Wang, J., Sharafi, C. S., McCoy, L. A., Naser, M. A., Ahmed, S., Sanders, K. L., Mohamed, A. S. R., Ding, Y., Wang, J., Hutcheson, K., Lai, S. Y., Fuller, C. D., & van Dijk, L. V. (2021). Intensity standardization methods in magnetic resonance imaging of head and neck cancer. *Physics and Imaging in Radiation Oncology*, *20*, 88–93. https://doi.org/10.1016/j.phro.2021.11.001

Woo, B., & Lee, M. (2021). Comparison of tissue segmentation performance between 2D U-Net and 3D U-Net on brain MR Images. *2021 International Conference on Electronics, Information, and Communication (ICEIC)*, 1–4. https://doi.org/10.1109/ICEIC51217.2021.9369797

Yaqoob, A., Musheer Aziz, R., & verma, N. K. (2023). Applications and Techniques of Machine Learning in Cancer Classification: A Systematic Review. *Human-Centric Intelligent Systems*, *3*(4), 588–615. https://doi.org/10.1007/s44230-023-00041-3

Zhao, Z., Cui, H., & Cui, H. (2025). Decoding tissue complexity: multiscale mapping of chemistry–structure–function relationships through advanced visualization technologies. *Journal of Materials Chemistry B*, *13*(27), 7897–7918. https://doi.org/10.1039/D5TB00744E

Zhou, C., Yang, X., Wu, S., Zhong, Q., Luo, T., Li, A., Liu, G., Sun, Q., Luo, P., Deng, L., Ni, H., Tan, C., Yuan, J., Luo, Q., Hu, X., Li, X., & Gong, H. (2022). Continuous subcellular resolution three-dimensional imaging on intact macaque brain. *Science Bulletin*, *67*(1), 85–96. https://doi.org/10.1016/j.scib.2021.08.003